ADVANCED INTELLIGENT SYSTEMS
Open Access
www.advintellsyst.com

Bioinspired Design, Fabrication, and Wing Morphing of 3D-Printed Magnetic Butterflies

Muhammad Bilal Khan, Kilian Schäfer,* Florian Hofmann, Matthias Lutzi, Eduardo Sergio Oliveros-Mata, Oleksandr Pylypovskyi, Denys Makarov, and Oliver Gutfleisch*

Monarch butterflies' remarkable migratory abilities, facilitated by their efficient wing structures, inspire the development of bioinspired soft robots and micro-aerial vehicles. This study presents the design, fabrication, and wing-morphing behavior of 3D-printed magnetic butterflies, focusing on optimal material and design parameters to replicate monarch wing-morphing behavior. Using composite of thermoplastic polyurethane and micron-sized $Nd_2Fe_{14}B$ magnetic powder, 12 unique butterfly designs—varying in size, vein patterns, and stiffness—are fabricated via powder bed fusion (PBF) 3D printing, resulting in 84 specimens. Lightweight and batch-producible with minimal postprocessing, the specimens have weights per unit area of ≈270, 480, and 1045 g m^{-2} for small, medium, and large sizes, respectively. A permanent magnet induces deformation in the specimens—mimicking monarch butterflies, without embedded electronics. A systematic analysis combining finite element simulations and experiments reveals the effects of size, geometric features, and laser energy scale on wing morphing. Lower laser energy scales result in porous, fast-bending specimens, while higher scales specimen show greater mechanical strength and varied deformation, with vein structures further improving deformation. The results provide a detailed dataset for optimizing wing-morphing designs while highlighting the potential of the PBF process in creating lightweight magnetic bioinspired structures capable of optimal shape morphing.

1. Introduction

The migratory behavior of monarch butterflies, enabled by their delicate and efficient wing structures, has long fascinated scientists and engineers.[1] These butterflies travel thousands of kilometers, demonstrating remarkable endurance and navigational skills.[1,2] The complex design and functionality of butterfly wings (**Figure 1**A,C), particularly their adaptability during flight, serve as a model for developing lightweight, flexible, and resource-optimal wings. Understanding and mimicking these natural wings could lead to the development of flexible wings with a wide range of controllability over fabrication parameters. Extensive research has explored butterfly morphology,[1] wing stiffness,[1,3] flight mechanics,[4–6] and migratory behaviors[1,7] to understand the key enablers of their flight capabilities.[8,9] A fundamental aspect of butterfly flight is the generation of aerodynamic forces through both active wing manipulation and the passive properties of wing deformability and shape.[4] The motivation for creating flexible wings lies in their ability to mimic the passive deformability observed in natural butterfly wings, which contributes significantly to their flight efficiency. Embedding detailed vein patterns and obtaining corresponding deformation profiles are crucial for developing wings that can adapt and respond to aerodynamic forces similarly to natural butterfly wings. Despite considerable research into developing systems capable of generating adequate aerodynamic forces, existing approaches often overlook sophisticated passive properties, such as wing deformation observed in natural butterfly

M. B. Khan, K. Schäfer, F. Hofmann, M. Lutzi, O. Gutfleisch
Functional Materials
Institute of Materials Science
Technical University Darmstadt
64287 Darmstadt, Germany
E-mail: Muhammad.khan3@tu-darmstadt.de;
Kilian.Schaefer@tu-darmstadt.de

The ORCID identification number(s) for the author(s) of this article can be found under https://doi.org/10.1002/aisy.202400620.

DOI: 10.1002/aisy.202400620

M. B. Khan, K. Schäfer, F. Hofmann, M. Lutzi, O. Gutfleisch
Additive Manufacturing Center
Technical University Darmstadt
64289 Darmstadt, Germany

E. S. Oliveros-Mata, O. Pylypovskyi, D. Makarov
Institute of Ion Beam Physics and Materials Research
Helmholtz-Zentrum Dresden-Rossendorf e.V.
01328 Dresden, Germany

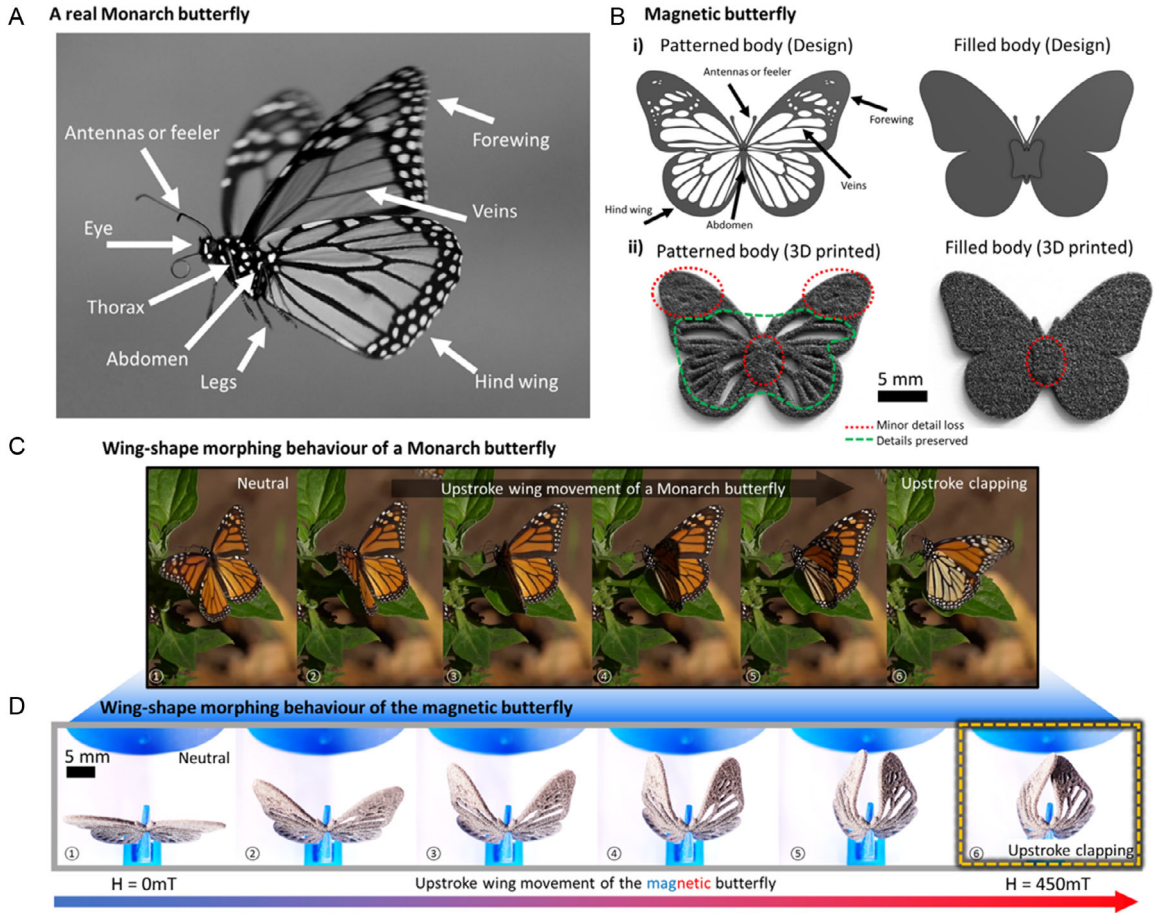

Figure 1. Bioinspired design and function of the magnetic butterfly. A) A photograph of a real monarch butterfly (courtesy of Dwight Sipler, reproduced under Creative Commons license 2.0) with labeled body parts, including the thorax, abdomen, legs, wings, veins, antennae, and eyes. B) An overview of the magnetic butterfly design, inspired by the morphology of real monarch butterflies. i) A labeled diagram illustrating the patterned body and filled body design of the magnetic butterfly. ii) A photograph of a 3D-printed magnetic butterfly showcasing the impact of various printing variables (as discussed in the main text) on the design's intricacies. C) A series of photographs depicting the wing-morphing behavior of a real monarch butterfly (©Evan Zucker). D) The magnetic butterfly wing-morphing behavior. The magnetic butterfly can be actuated to simulate the upstroke wing clapping, a crucial wing-morphing mechanism employed by monarchs to generate lift and thrust, among other complex maneuvers.

wings, limiting their effectiveness and versatility in real-world applications. This gap can be attributed to the limitations of previously used materials and fabrication techniques. For example, the USTButterfly robot mimicked butterfly flight using wings made of carbon rods and chlorinated polyethylene,[10] while another study used Kapton film reinforced with carbon rods.[11] DelFly Micro employed Mylar foil wings with electrical actuation.[12] These materials and methods, while innovative, often resulted in rigid components or complex fabrication procedures prone to manufacturing errors, leading to bulkier designs with limited compliance behavior and high energy consumption. To address these challenges, recent developments in 3D printing and soft robotics[13–38] offer opportunities to mass-produce compliant structures made of flexible materials capable of shape morphing. Among various flexible materials used in 3D printing, such as thermoplastic elastomers, silicone-based polymers, shape memory polymers, and hydrogels, magnetic composites are notable for their unique magnetic and mechanical properties.[26,32,36] Magnetic composites incorporate magnetic fillers within a polymer matrix, allowing the material to respond dynamically to external magnetic fields.[36] This capability makes them particularly suitable for fabricating morphing structures like butterfly wings. The unique properties of magnetic composites enable remote and noiseless operation, as well as passive-active compliance, where the polymer matrix deforms passively while the embedded magnetic particles actively respond to magnetic stimuli. These features are being actively explored for a range of applications, including bioinspired sensors, actuators, and complex, adaptive shapes developed through additive manufacturing.[25,26,32,38,39] Among various 3D printing techniques, such as stereolithography and fused deposition modeling, powder bed fusion (PBF) allows for printing magnetic composites with precise control over the composite density and corresponding porosity at each instance of printing.[40,41] This makes PBF ideal for fabricating multifunctional composites with intricate designs, flexibility gradients, and embedded features. The method offers further tunability of mechanical properties through variations in laser energy, enabling precise adjustments

within and across printed batches. This precision is crucial for creating structures that require fine control over stiffness gradients and geometric features, such as butterfly wings.

This study presents a systematic approach to design, fabricate, and analyze the wing morphing (Figure 1D) of 3D-printed magnetic butterflies in a static actuation setup, drawing inspiration from monarch butterfly wing behavior (Figure 1C). Magnetic butterfly specimens are evaluated based on defined shape-morphing criteria, focusing on the ability to perform a full upstroke clapping—a mechanism crucial for lift and thrust generation in real monarch butterflies. Using a magnetic composite composed of thermoplastic polyurethane (TPU) and $Nd_2Fe_{14}B$ permanent magnetic powder, twelve distinct butterfly designs (**Figure 2**A,B) are fabricated via PBF 3D printing (also known as 4D printing for shapes that change from under a stimulus).[23,40,41] These designs, varying in size, embedded thin vein patterns, and stiffness, are systematically evaluated under magnetic field stimuli, resulting in 84 specimens for analysis. The comprehensive analysis combines finite element simulations and experimental validations, showing the effects of key parameters—such as size, geometric features, and laser energy scale (a fabrication parameter representing the laser energy)—on wing-morphing behavior. This approach enables a systematic investigation and optimization of material and design parameters, laying the groundwork for the development of agile, efficient, and versatile flexible wings, with potential applications in magnetic soft robotics and micro aerial vehicles. This study shows the potential of utilizing magnetic composites and PBF 3D printing as a robust method for creating bioinspired, flexible, and magnetically actuated structures for soft robotics.

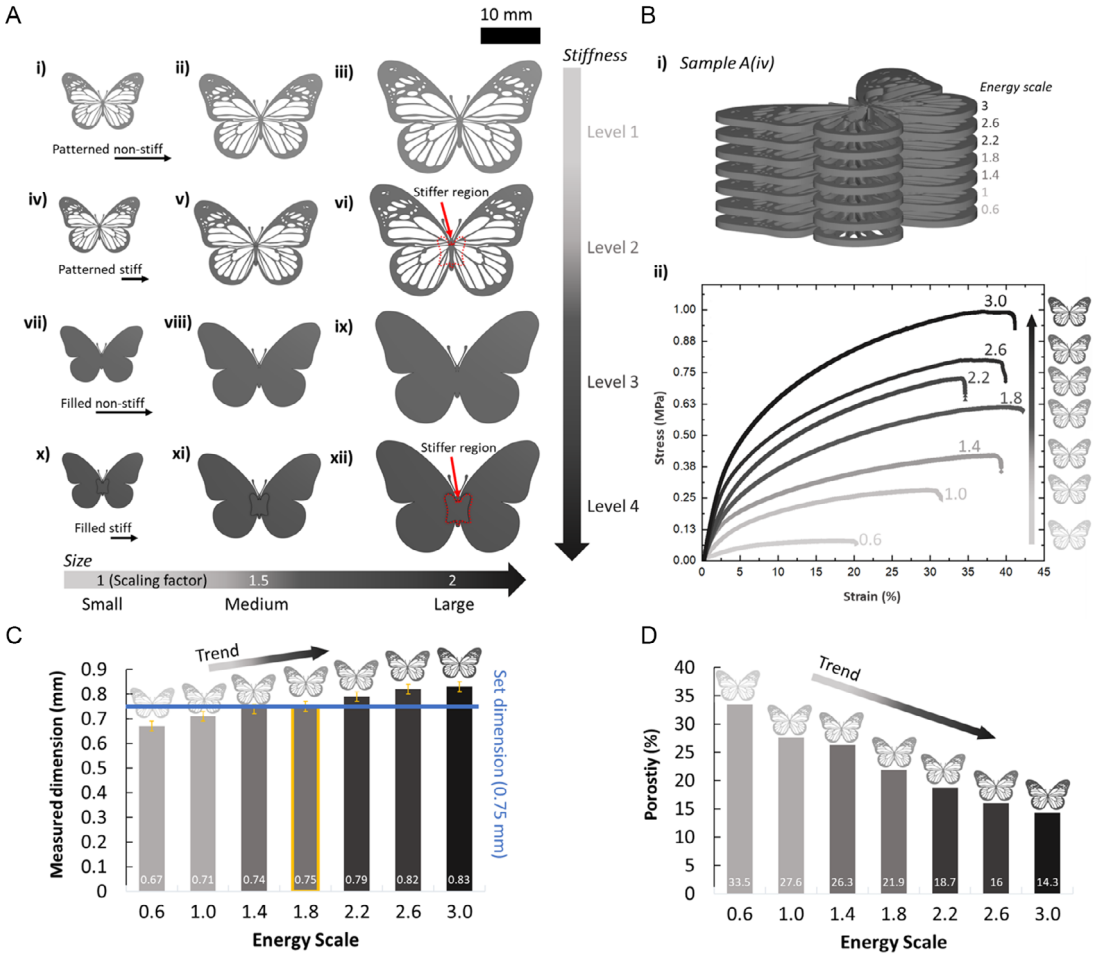

Figure 2. Parameters for designing and investigating magnetic butterfly fabrication. A) Twelve designs showcasing variations in size and embedded stiffness through geometric features. i–iii) Three sizes (small, medium, large) of a patterned butterfly with intricate embedded vein structures. iv–vi) Three sizes (small, medium, large) of the same patterned design with an additional geometric feature, increasing stiffness in the central region between the wings on both sides of the magnetic butterfly. vii–xii) Filled magnetic butterfly shapes with embedded vein patterns in three sizes, with and without the stiffer central region between the wings. B) The effect of laser energy scale on the tensile properties of the magnetoactive composite. i) A view of the PBF printing file showing seven specimen of the patterned magnetic butterfly stacked with varying laser energy scales as indicated. ii) Tensile stress–strain curves of the magnetoactive composites, illustrating the impact of the laser energy scale parameter on the specimen produced. C) A graph showing the effect of the laser energy scale parameter on the dimensions of the produced specimen, indicating consistent variation except for the 1.8 laser energy scale specimen, which came out as designed after printing. D) A graph displaying the effect of variations in the laser energy scale parameter on the porosity of the specimen, with lower laser energy scale values resulting in higher porosity and vice versa.

2. Experimental Section

2.1. Materials

In this study, we used TPU powder (20–105 μm particle size) from Sinterit, Poland, as the binder, and $Nd_2Fe_{14}B$ permanent magnetic powder (35–55 μm particle size) MQP-S from Neo Magnequench, Singapore, as the filler. The MQP-S powder has a spherical particle shape. The specific properties of the used materials are provided in Table S1 (Supporting Information).

2.2. Production of the Magnetic Composite

The magnetic composite was produced by mechanically mixing TPU and MQP-S powders, following the method described in ref. [39]. The mixing was conducted for one hour using a mechanical mixer from WAB-GROUP, Switzerland. The composite consisted of 50% by weight of MQP-S, corresponding to an approximate volume fraction of 12.7%.

2.3. Fabrication of the Magnetic Butterflies

The magnetic butterflies were 3D-printed using the magnetic composite powder and a Lisa Pro printer from Sinterit, Poland. This printer utilizes the PBF technique, an additive manufacturing process that uses a laser to sinter powdered material, binding it together to create a solid structure. Detailed printer settings are listed in Table S2 (Supporting Information). The printer has the capacity to print all 86 specimens in a single print job, with additional space for larger batches. After printing, the specimens were thoroughly cleaned using compressed air to remove any residual powder particles. The dimensions of the printed specimen were measured using a verneir caliper. The porosity of the magnetic composite printed with varying laser energy scales (defined by the manufacturer to vary from 0.6 (low) to 3.0 (high)) was obtained by the ratio of the geometrical density to the theoretical density for a completely dense composite.

2.4. Characterization of the Magnetic Composites

The tensile properties of the magnetic composite were evaluated in accordance with ASTM D638 standards. For each laser energy scale parameter, five type IV dumbbell-shaped samples were produced. Mechanical testing was performed using an Inspekt Table 5 (Hegewald and Peschke, Germany), equipped with a 100 N load cell, at a test speed of 5 mm min^{-1}. Strain measurements were based on the displacement of the traverse, with a grip distance set at 32.5 mm. The magnetic properties of the composites were assessed using cube-shaped samples with a side length of 7.5 mm to ensure standardized geometries, thereby eliminating geometric influences on the hysteresis loops as magnetic properties are normalized to the specimen's volume. A HyMPulse pulsed-field magnetometer was utilized to evaluate samples processed at different laser energy scales. The magnetic hysteresis loop, initial magnetization curve of the MQP-S powder, and the second quadrant demagnetization curves for the magnetic composites are summarized in Figure S2 (Supporting Information). As porosity decreases with higher laser energy scales, the remanence of the magnetic composites increases from 47 to 76 mT. Although the theoretical remanence for fully dense samples is 92 mT, the 14.3% porosity in the sample produced at a laser energy scale of 3.0 results in a measured remanence close to 76 mT. Coercivity remains consistent at around 885 mT for samples produced with higher laser energy scales. Slight decreases in coercivity are observed at laser energy scales of 0.6 and 1.0 due to weaker particle embedding and potential rotation during demagnetization, impacting actuation efficiency.[39]

2.5. Finite Element Simulations

Finite element simulations were conducted to evaluate the wing-morphing behavior and stress distribution of the butterfly specimens under specified force loads. Computer-aided design (CAD) models of the butterflies were created using Onshape (PTC, U.S.), resulting in four designs each scaled to small, medium, and large dimensions, totaling 12 variants. Exact dimensions and average weights of all designs and sizes are listed in **Table 1**. Simulations were performed using ANSYS Mechanical (Release 2023-R2, Ansys, U.S.), employing a nonlinear static structural solver to account for large deformations and nonlinear material behavior inherent in the magnetoactive composites. The material properties were defined using the Mooney–Rivlin three-parameter hyperelastic model, fitted based on experimental tensile data (Figure 2B), to capture the material's nonlinear stress–strain relationship and finite deformation behavior. The specimens were meshed with tetrahedral quadratic elements (SOLID285), using an element size of 0.1 mm to balance computational efficiency and accuracy in capturing deformation variations. For example, the mesh for the large specimen consisted of ≈77 811 nodes and 347 196 elements. Mesh density was adjusted proportionally for medium and small specimens to maintain consistency across models. Boundary conditions were applied by fixing the center of the butterfly (representing the body) in space to simulate the attachment point during actuation, allowing the wings to deform freely under applied loads. Uniform surface loads were applied across the wing surfaces to emulate the magnetic force interaction, replicating the experimental conditions where the wings bend upward in response to magnetic forces. The load was applied to the bottom surface of the butterflies, causing upward wing bending. Load values were iterated—by incrementally increasing the applied force—until complete wing bending was achieved. These values were then used to compare additional loading effects on other designs. Convergence criteria

Table 1. Dimensions and weight per unit area measurements of various butterfly specimens. Length and width are based on bounding box measurements of the magnetic butterfly specimens.

Specimen	Length [mm]	Width [mm]	Thickness [mm]	Weight per unit area [g m^{-2}]
Small	13.81	9.47	0.75	270
Medium	20.71	14.21	0.75	480
Large	27.62	18.94	0.75	1045

were set using default ANSYS settings, with displacement convergence at 0.5%. Convergence was ensured by monitoring residuals and verifying that equilibrium iterations satisfied the energy norms. The simulations converged successfully, and the solver output confirmed that the solution met the required criteria. These parameters and settings are summarized in Table S3 (Supporting Information).

2.6. Shape Programming and Characterization of Butterfly Wing-Morphing Behavior

To magnetize the butterfly specimens to different profiles, we used polylactic acid-based 3D-printed shape templates. The "profile" refers to the wing position during magnetization. Various magnetization profiles were tested, but the out-of-plane magnetization profile was used for all specimens in this study to achieve the maximum stroke angle. Fixing the wing position of the magnetic butterflies at a predefined stroke angle during magnetization confines the wing movement within this defined range. Figure S2C, Supporting Information shows three representative magnetization profiles.

For actuation, we utilized a permanent magnet setup involving a NdFeB permanent magnet mounted onto a custom 3D-printed movable platform (Figure 4D). The magnetic butterfly specimen was clamped on top between the wings. By moving the magnet toward and away from the specimen, the butterfly wings responded to the magnetic field, transitioning from a fully deformed (upstroke clapping) state to an undeformed (neutral) state. A custom-made magnetic field scanner based on a Hall effect sensor measured the magnetic field variation with changing distance from the magnet. Additionally, a digital camera (Sony Cyber-shot DSC-RX100 V) captured photos and videos during actuation. Image processing methods were applied to analyze the data and obtain wing-shape deformation values. These values facilitated the comparison of specimen performance based on a predefined criterion, allowing for uniform evaluation of all specimens' ability to perform upstroke clapping.

To study the wing-morphing behavior of the magnetic butterflies, we combined simulations with experimental characterization. In our simulations, magnetic actuation was simplified by applying equivalent force loads across the wing surfaces. These forces were derived from measurements of the magnetic force exerted by the permanent magnet at various distances corresponding to the experimental magnetic fields. For large specimens, forces of ≈20 mN for unfilled designs and 0.5 N for filled designs were applied to achieve full wing clapping, corresponding to a magnetic field of up to 450 mT. Loads were increased incrementally—by 0.1 mN for unfilled specimens and 0.1 N for filled specimens—until the desired deformation was achieved. Due to the nonuniform magnetic field of the permanent magnet in experiments, the deformation behavior is not exactly the same as in the simulated load conditions. The nonuniform field causes variable wing deformation but still guarantees wing clapping. Examination of the experimental deformation angles (Figure 4B) showed that all large specimens achieved wing bending angles exceeding 90 degrees under magnetic stimuli of up to 450 mT, confirming the clapping behavior. Although simulated deformation values did not exactly match experimental values, the simulations demonstrated wings deforming beyond the clapping point, consistent with observations where wings bend over 90 degrees. Discrepancies are within acceptable limits and are attributed to factors such as magnetic field nonuniformity and simulation simplifications. Importantly, both simulations and experiments confirm that the wings can bend to 90 degrees and beyond under magnetic stimuli of up to 450 mT. An analysis comparing deformation results from force application with experimental measurements confirmed the validity of our approach (see Table S4, Supporting Information).

3. Results and Discussion

3.1. Design and Fabrication of the Magnetic Butterflies

The design of the magnetic butterflies was inspired by the morphology of monarch butterflies, featuring vein structures and similar dimensions. Figure 2A displays twelve designs, highlighting variations in size and geometric details. To evaluate the effect of size on wing deformation, wing lengths of 8, 12, and 16 mm were considered for small, medium, and large wings, respectively. The designs also included subcategories with different embedded features, which either reduced mass (patterned specimens) or increased mass (filled designs with stiffer or nonstiff center regions), creating variability in topological stiffness as a sub-parameter for evaluating deformation during magnetic stimulation. The butterflies were fabricated using a magnetic composite of MQP-S and TPU via a PBF process, which employs a laser to sinter powdered material into a solid structure. This method resulted in one-piece functional butterflies without additional parts. The tensile properties of composites printed with varying laser energy scales (0.6–3.0) indicated that the laser energy scale strongly affects material binding during laser sintering. Figure 2 illustrates the designs, tensile properties, variations between designed and printed dimensions, and porosity changes with different laser energy scales. All butterfly specimens were set to a thickness of 0.75 mm, with only length and width scaled to create small, medium, and large specimens. The laser energy scale, representing the energy transferred to the powder bed, affected the quality of printed details (Figure S1, Supporting Information). It caused minor shrinkage in the printed specimens at lower energy scales (0.6, 1.0, and 1.4) and expansion at higher energy scales (2.2, 2.6, and 3.0). At a laser energy scale of 1.8, however, the specimen matched the design specifications precisely, demonstrating the optimal laser power parameter for printing dimension-sensitive parts (Figure 2C). Higher laser energy scales increased density and reduced porosity in the specimens, as shown in Figure 2D. In contrast, lower laser energy scales led to higher porosity. Specifically, the highest energy scale produced specimens with a porosity of 14.3%, while the lowest energy scale resulted in a porosity of 33.5%, demonstrating a difference of ≈57.3% in porosity between the highest and lowest energy scales. Surface roughness also varied, with more porous specimens preserving finer details (Figure S1, Supporting Information). Moreover, larger specimens exhibited clearer feature definitions and bent more easily due to less stiffness compared to smaller, stiffer specimens.

3.2. Simulation and Realization of the Upstroke Clapping of the Magnetic Butterfly Wings

Finite element analysis (FEA) on the butterfly designs showed that patterned butterflies required less force to deform for upstroke wing-clapping compared to filled specimens. **Figure 3** presents FEA results, showing deformation and von Mises stress distribution on the specimens. For simplicity, we use specific notations to identify the specimens: "U" for unfilled specimens, "U-S" for unfilled specimens with embedded stiffness regions, "F" for filled specimens, and "F-S" for filled specimens with embedded stiffness regions between the magnetic wings, respectively. The FEA results for large (U) specimens indicated significant deformation (13.54 mm under 5 mN load and 21.37 mm under 20 mN load) with associated stresses (0.12 and 0.32 MPa, respectively). The large (U-S) specimens showed reduced deformation and stress compared to the large (U) specimens due to the added stiffness. Filled designs (F and F-S) required higher loads (0.1 and 0.5 N) for similar deformations, indicating their increased stiffness and resistance to bending.

3.3. Wing-Morphing Behavior of the Magnetic Butterflies

A total of 84 magnetic butterfly specimens were fabricated and evaluated for their wing deformation behavior upon magnetic actuation. **Figure 4** provides an overview of the experimental evaluation for a selected group of magnetic butterflies printed at laser energy scale of 1.4. The following sections discuss the parameters impacting wing deformation.

3.3.1. Effect of Size on Wing-Morphing Behavior

The size of the butterflies significantly influenced their wing-morphing behavior. Larger specimens exhibited more significant deformation due to their less stiff geometry, allowing easier bending compared to smaller, stiffer specimens. For instance, the large (U) specimen demonstrated a deformation of 15.6 mm, whereas the small (U) specimen showed 6.9 mm deformation (Figure 4A,B). This means a size increase by a factor of two resulted in a 126% increase in deformation by direct non-scaled deformation comparison. This size effect was consistent across all specimens, as observed in both simulations and actual magnetic actuation tests. However, discrepancies between simulated and experimental deformation modes were noted, specifically the mid-wing bending observed experimentally but not in simulations. These differences can be attributed to the nonuniform magnetic field generated by the permanent magnet. To avoid repetition of data, only key representative simulation and experimental results are included in this paper.

3.3.2. Effect of Geometric Features

Geometric features, such as vein structures and stiffer regions between the wings, played a crucial role in deformation behavior. Specimens with vein structures deformed faster and required less force, showing higher levels of deformation compared to those without vein structures. For example, the large (U) specimen had larger deformation (15.6 mm) compared to the large (F) specimen (17.9 mm). Vein structures contributed to a 14.7% increase in deformation efficiency. In specimens with both vein structures and stiffer regions, the vein structures dominated the deformation behavior. In contrast, in filled specimens without vein structures, the addition of a stiffer center region restricted bending.

3.3.3. Effect of Varying Laser Energy Scale

The laser energy scale parameter affected the deformation behavior. Specimens printed at an energy scale of 0.6 preserved finer details (Figure S1A, Supporting Information) but were more fragile due to higher porosity, resulting in maximum and faster bending upon magnetic stimulation but were prone to mechanical damage. Higher laser energy scale specimens (3.0) had lower porosity and were mechanically stronger (Figure S1B, Supporting Information), showing variable deformation behavior depending on size and pattern features. For example, the large (U) specimen showed a deformation of 15.6 mm at an energy scale of 1.4, whereas specimens at higher laser energy scales exhibited less deformation due to increased stiffness. Overall, the laser energy scale controlled bending performance, with a tradeoff between mechanical strength and deformation, influenced by size and geometric features.

3.4. Key Insights and Future Directions

The study demonstrates that size, geometric features, and laser energy scale are essential parameters influencing wing-morphing behavior of 3D-printed magnetic butterfly specimens. Larger specimens with vein structures and lower laser energy scales showed larger deformation, providing baseline data for further research. The upstroke clapping was reproduced, showing that wing clapping is not surface-to-surface; rather, the forewings could fold to mimic it, creating a wide flight envelope. Future work should incorporate machine learning approaches[42] to optimize the design of magnetically actuated flexible structures for applications like bioinspired flight and thrust generation. The results suggest potential for fabricating magnetically actuated structures with minimal post-processing and embedded geometric features that passively result in desired wing-morphing behavior.

While our artificial butterflies replicate morphological and stiffness characteristics of real butterflies, their weight and density for real flight will be examined in future studies through testing in dynamic magnetic fields. Future considerations may include design strategies such as internal lattice structures to reduce mass. As an additional insight while recognizing the importance of fatigue performance for applications involving repetitive wing actuation, preliminary fatigue tests were conducted using two methods. First, specimens were mounted in a homogeneous magnetic coil setup and subjected to repeated cycles of low and high-frequency wing movements. After 100 cycles, no fatigue or degradation was observed (see Movie S1, Supporting Information). Second, specimens were repeatedly actuated using a permanent magnet, with no signs of fatigue after multiple cycles. Specimens fabricated at the lowest energy scale (0.6) exhibited fragility under high-frequency actuation.

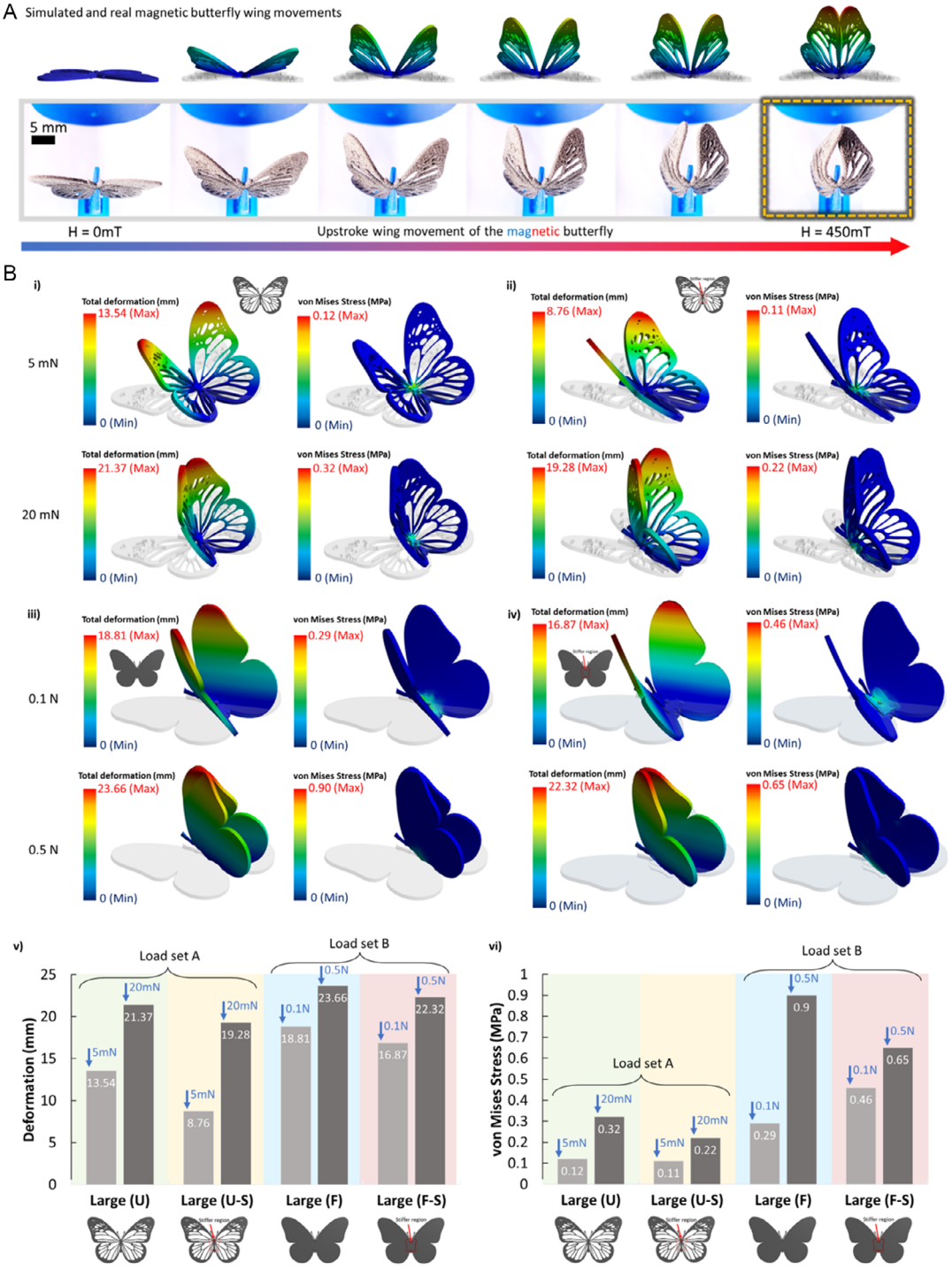

Figure 3. Evaluation of deformation and stress behavior for the twelve butterfly designs through finite element simulations. A) Simulation snippets showing the magnetic butterfly wing clapping behavior during the upstroke and the deformation regions in the wings. The top row shows simulated images, while the bottom row presents photographs of the fabricated magnetic butterfly under varying magnetic fields, ranging from 0 mT in the neutral upstroke position to fully folded wings in the upstroke at 450 mT stimuli provided by a permanent magnet. B) Finite element simulation of the different butterfly designs under various loads applied incrementally. For the patterned design magnetic butterflies, loads ranged from 5 to 20 mN, whereas higher loads of 0.1 and 0.5 N were applied to the filled designs. Larger sizes exhibited greater deformation. Additionally, stiff designs showed less deformation compared to nonstiff designs. Patterned designs required significantly less force (e.g., 5 mN) to achieve the desired wing clapping compared to filled designs, which required higher force for the same bending effect. i–iv) Simulation snippets illustrating these behaviors. v–vi) Comparative graphs showing the deformation and von Mises stress evaluated through FEA of the composite, respectively.

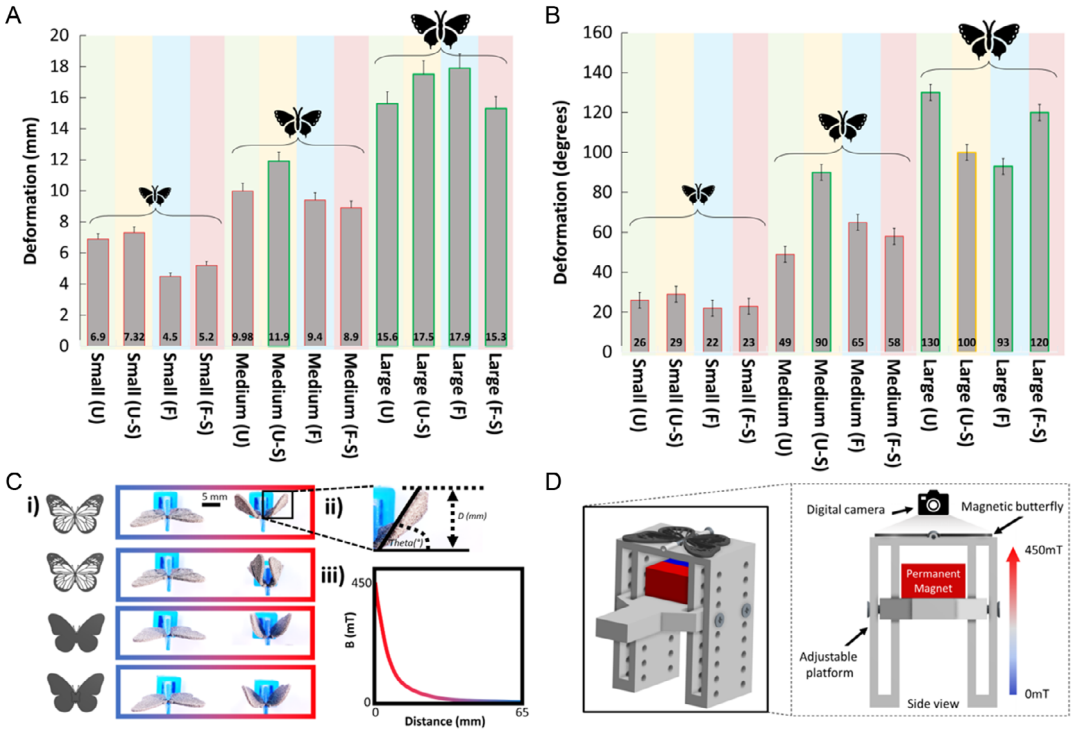

Figure 4. Experimental evaluation of the wing-morphing behavior of magnetic butterflies. A,B) Graphs illustrating deformation measured in millimeters and degrees, respectively, for each butterfly specimen shown here produced with laser energy scale 1.4. Notations "U", "U-S", "F", and "F-S" denote unfilled specimen, unfilled with embedded stiffness region, filled specimen, and filled with embedded stiffness region, between the magnetic butterfly wings, respectively. C) i) Representative images of small-sized magnetic butterfly specimens (laser energy scale 1.4) in various neutral and deformed states, each specimen responding differently to magnetic stimuli. ii) Method for experimentally measuring butterfly wing deformation, with "d" representing deformation from a marked position and "theta" denoting the angle formed between the horizontal axis and the wing tip upon deformation. iii) A graph showing the magnetic field variation of the permanent magnet with varying distance from a mounted magnetic butterfly specimen. D) Schematic of the experimental setup employing a permanent magnet to actuate the magnetic butterfly specimen held within a specifically designed platform (Images not on the actual scale).

These observations suggest that specimens maintain performance after many cycles, particularly those fabricated at higher energy scales. We plan to investigate this systematically in future studies, focusing on long-term fatigue performance.

Currently, our designs produce primarily upward and downward wing motions due to the symmetric out-of-plane magnetic field application. However, the structure allows for potential flexibility to achieve more complex movements. To replicate these complex wing movements, we plan to explore magnetic field configurations that include an additional in-plane component. By applying a magnetic field that changes direction at specific timings, we aim to control the wings' forward and backward motions. Future studies will focus on implementing tilted magnetic sources, differential actuation, or time-varying magnetic fields with controlled directionality to achieve this enhanced wing flexibility. Additionally, the current experimental setup is used for static evaluation of deformation behavior. Evaluation of lift,[6] thrust, and symmetric wing stroke combinations for dynamic flight are the next steps. Patterned specimens will be modified to incorporate nonmagnetic thin foils in the patterned areas to achieve whole-body thrust. In this design, the magnetic composite structure will act as a skeleton or muscle-like actuation mechanism underneath the foils. To dynamically evaluate the butterflies under varying magnetic field amplitudes and actuation frequencies, setups based on paired coils[43] are planned. The goal will be to utilize a uniform alternating magnetic field with controllable parameters, allowing the butterflies to fly along a straight path between two predetermined points in a laboratory setting. Additionally, different magnetization profiles for the wings and body for posture control during flight, as well as the suitability of better magnetically performing materials for energy-efficient actuation,[44,45] will be explored.

4. Conclusion

This study explores the design, fabrication, and wing-morphing behavior of 3D-printed magnetic butterflies, inspired by the morphology and wing movement of monarch butterflies. Using a magnetic composite material composed of TPU and $Nd_2Fe_{14}B$-based magnetic powder, twelve distinct butterfly designs were created through PBF 3D printing. The material properties were evaluated, confirming their suitability for fabricating flexible magnetic butterflies. Finite element simulations and experimental validations were conducted to investigate the influence of key parameters such as size, geometric features, and laser energy scale on

wing-morphing behavior. The results show that these parameters, along with the PBF process, provide a valuable foundation for developing flexible, magnetically actuated structures capable of compliant shape morphing. Our findings highlight the potential of PBF in creating dynamic, lightweight structures with sophisticated shape-morphing capabilities. Specimens produced at lower laser energy scales exhibited higher porosity and faster bending responses, while those produced at higher laser energy scales demonstrated greater mechanical strength with varied deformation characteristics. This comprehensive dataset offers valuable insights for optimizing wing-morphing designs and lays the groundwork for future advancements in bioinspired aerial vehicle development. Currently, the actuation of the magnetic butterflies was performed solely to evaluate wing morphing under static conditions. To fully investigate essential flight parameters such as lift and thrust generation, future work will need to evaluate these factors dynamically. This will include assessing the flight performance of the most suitably deforming magnetic butterflies and their corresponding aerodynamic characteristics. Additionally, future work will involve using existing data to develop a data-driven machine learning approach, expanding the knowledge base for optimal design scaling by incorporating further studies on lift and thrust generation.

While the focus of the study was to fabricate flexible magnetic wings, the approach can be extended to various other shape-morphing robots.[29–35] By using the presented approach, magnetic composite-based 3D printed assemblies with optimally incorporated flexibility gradients can be integrated into these robots, replacing traditionally cast assemblies. This enables the creation of multi-material, precisely manufactured, morphing structures that leverage different printing technologies and materials. This approach can contribute to creating optimal synergies between bioinspired shape design, materials, control, and utilization for improved performance of shape-morphing robots.

Supporting Information

Supporting Information is available from the Wiley Online Library or from the author.

Acknowledgements

This work was financially supported by the Deutsche Forschungsgemeinschaft (DFG, German Research Foundation), Project ID No. 405553726, TRR 270, and the RTG 2761 LokoAssist (grant no. 450821862).

Conflict of Interest

The authors declare no conflict of interest.

Author Contributions

Muhammad Bilal Khan: Conceptualization (lead); Data curation (lead); Formal analysis (lead); Investigation (lead); Methodology (lead); Validation (lead); Visualization (lead); Writing—original draft (lead). **Kilian Schäfer**: Conceptualization (supporting); Resources (supporting); Writing—review & editing (equal). **Florian Hofmann**: Resources (supporting); Writing—review & editing (supporting). **Matthias Lutzi**: Resources (supporting); Writing—review & editing (supporting). **Eduardo Sergio Oliveros-Mata**: Investigation (supporting); Writing—review & editing (supporting). **Oleksandr Pylypovskyi**: Investigation (supporting); Writing—review & editing (supporting). **Denys Makarov**: Supervision (supporting); Writing—review & editing (equal). **Oliver Gutfleisch**: Funding acquisition (lead); Supervision (lead); Writing—review & editing (equal).

Data Availability Statement

The data that support the findings of this study are available from the corresponding author upon reasonable request.

Keywords

4D printing, bioinspired robotics, magnetic composites, shape morphing

Received: July 25, 2024
Revised: November 11, 2024
Published online:

[1] C. Le Roy, V. Debat, V. Llaurens, *Biol. Rev.* **2019**, *94*, 1261.
[2] M. Kovac, D. Vogt, D. Ithier, M. Smith, R. Wood, in *2012 IEEE/RSJ Inter. Conf. on Intelligent Robots and Systems*, October **2012**, pp. 1102–1109, https://doi.org/10.1109/IROS.2012.6385453.
[3] S. J. Steppan, S. J. Steppan, *J. Res. Lepid.* **2000**, *35*, 61.
[4] C. R. Betts, R. J. Wootton, *J. Exp. Biol.* **1988**, *138*, 271.
[5] K. Berwaerts, E. Matthysen, H. Van Dyck, *Evolution* **2008**, *62*, 2525.
[6] R. B. Srygley, A. L. R. Thomas, *Nature* **2002**, *420*, 660.
[7] S. Altizer, A. K. Davis, *Evolution* **2010**, *64*, 1018.
[8] D. Floreano, R. J. Wood, *Nature* **2015**, *521*, 460.
[9] C. Zhang, C. Rossi, *Bioinspir. Biomim.* **2017**, *12*, 025005.
[10] H. Huang, W. He, Y. Zou, Q. Fu, *IEEE Trans. Ind. Electron.* **2024**, *71*, 1758.
[11] S. Miyasaka, C. Kang, H. Aono, *Sens. Mater.* **2023**, *35*, 3097.
[12] G. C. H. E. de Croon, K. M. E. de Clercq, R. Ruijsink, B. Remes, C. de Wagter, *Int. J. Micro Air Veh.* **2009**, *1*, 71.
[13] Y. Kim, X. Zhao, *Chem. Rev.* **2022**, *122*, 5317.
[14] T. Li, G. Li, Y. Liang, T. Cheng, J. Dai, X. Yang, B. Liu, Z. Zeng, Z. Huang, Y. Luo, T. Xie, W. Yang, *Sci. Adv.* **2017**, *3*, e1602045.
[15] E. S. Oliveros-Mata, R. Xu, L. Guo, D. Makarov, *Phys. Rev. Appl.* **2023**, *20*, 060501.
[16] E. Sachyani Keneth, A. Kamyshny, M. Totaro, L. Beccai, S. Magdassi, *Adv. Mater.* **2021**, *33*, 2003387.
[17] T. J. Wallin, J. Pikul, R. F. Shepherd, *Nat. Rev. Mater.* **2018**, *3*, 84.
[18] Y. Lee, F. Koehler, T. Dillon, G. Loke, Y. Kim, J. Marion, M.-J. Antonini, I. C. Garwood, A. Sahasrabudhe, K. Nagao, X. Zhao, Y. Fink, E. T. Roche, P. Anikeeva, *Adv. Mater.* **2023**, *35*, 2301916.
[19] R. Pramanik, R. W. C. P. Verstappen, P. R. Onck, *Appl. Phys. Rev.* **2024**, *11*, 021312.
[20] L. Ning, C. Limpabandhu, Z. T. H. Tse, *Soft Robot.* **2024**, *11*, 2.
[21] Z. Li, Y. P. Lai, E. Diller, *Adv. Intell. Syst.* **2024**, *6*, 2300052.
[22] J. Yao, Q. Cao, Y. Ju, Y. Sun, R. Liu, X. Han, L. Li, *Adv. Intell. Syst.* **2023**, *5*, 2200339.
[23] L. Joharji, R. B. Mishra, F. Alam, S. Tytov, F. Al-Modaf, N. El-Atab, *Microelectron. Eng.* **2022**, *265*, 111874.
[24] Y. Kim, H. Yuk, R. Zhao, S. A. Chester, X. Zhao, *Nature* **2018**, *558*, 274.
[25] P. Zhu, W. Yang, R. Wang, S. Gao, B. Li, Q. Li, *ACS Appl. Mater. Interfaces* **2018**, *10*, 36435.

[26] X. Wei, M.-L. Jin, H. Yang, X.-X. Wang, Y.-Z. Long, Z. Chen, *J. Adv. Ceram.* **2022**, *11*, 665.
[27] X. Wang, G. Mao, J. Ge, M. Drack, G. S. Cañón Bermúdez, D. Wirthl, R. Illing, T. Kosub, L. Bischoff, C. Wang, J. Fassbender, M. Kaltenbrunner, D. Makarov, *Commun. Mater.* **2020**, *1*, 1.
[28] J. Sun, B. Tighe, Y. Liu, J. Zhao, *Soft Robot.* **2021**, *8*, 213.
[29] J. Sun, E. Lerner, B. Tighe, C. Middlemist, J. Zhao, *Nat. Commun.* **2023**, *14*, 6023.
[30] L. Wang, Y. Chang, S. Wu, R. R. Zhao, W. Chen, *Nat. Commun.* **2023**, *14*, 8516.
[31] Y. Alapan, A. C. Karacakol, S. N. Guzelhan, I. Isik, M. Sitti, *Sci. Adv.* **2020**, *6*, eabc6414.
[32] V. G. Kortman, E. de Vries, J. Jovanova, A. Sakes, *3D Print. Addit. Manuf.* **2024**, *11*, 977.
[33] A. K. Bastola, M. Hossain, *Mater. Des.* **2021**, *211*, 110172.
[34] S. Leanza, S. Wu, X. Sun, H. J. Qi, R. R. Zhao, *Adv. Mater.* **2024**, *36*, 2302066.
[35] Y. Liu, G. Lin, M. Medina-Sánchez, M. Guix, D. Makarov, D. Jin, *ACS Nano* **2023**, *17*, 8899.
[36] S. Wu, W. Hu, Q. Ze, M. Sitti, R. Zhao, *Multifunct. Mater.* **2020**, *3*, 042003.
[37] A. Kirillova, L. Ionov, *J. Mater. Chem. B* **2019**, *7*, 1597.
[38] I. Apsite, S. Salehi, L. Ionov, *Chem. Rev.* **2022**, *122*, 1349.
[39] K. Schäfer, M. Lutzi, M. B. Khan, L. Schäfer, I. Dirba, S. Bruns, I. Valizadeh, O. Weeger, C. Hartmann, M. Kupnik, E. Adabifiroozjaei, L. Molina-Luna, K. Skokov, O. Gutfleisch, *Addit. Manuf.* **2024**, *79*, 103905.
[40] K. Schäfer, T. Braun, S. Riegg, J. Musekamp, O. Gutfleisch, *Mater. Res. Bull.* **2023**, *158*, 112051.
[41] K. Schäfer, R. G. T. Fim, F. Maccari, T. Braun, S. Riegg, K. P. Skokov, D. Koch, E. Bruder, I. Radulov, C. H. Ahrens, P. A. P. Wendhausen, O. Gutfleisch, *J. Magn. Magn. Mater.* **2023**, *583*, 171064.
[42] J. Hiller, H. Lipson, *IEEE Trans. Robot.* **2012**, *28*, 457.
[43] Z. Yang, L. Zhang, *Adv. Intell. Syst.* **2020**, *2*, 2000082.
[44] L. Han, F. Maccari, I. R. Souza Filho, N. J. Peter, Y. Wei, B. Gault, O. Gutfleisch, Z. Li, D. Raabe, *Nature* **2022**, *608*, 310.
[45] O. Gutfleisch, M. A. Willard, E. Brück, C. H. Chen, S. G. Sankar, J. P. Liu, *Adv. Mater.* **2011**, *23*, 821.